Supplementary Information

Organometal halide perovskite supported Pt single-atom photocatalyst for H_2 evolution

Yaqiang Wu[a], Qian Wu[b], Qianqian Zhang[a], Zaizhu Lou[c], Kefeng Liu,[a] Yandong Ma[b], Zeyan Wang[a], Zhaoke Zheng[a], Hefeng Cheng[a], Yuanyuan Liu[a], Ying Dai[b], Baibiao Huang[a], Peng Wang[a]*

[a]State Key Laboratory of Crystal Materials, Shandong University, Jinan 250100, China

[b]School of Physics, Shandong University, Jinan 250100, China

[c]Institute of Nanophotonics, Jinan University, Guangzhou, 511443, China

*e-mail: pengwangicm@sdu.edu.cn

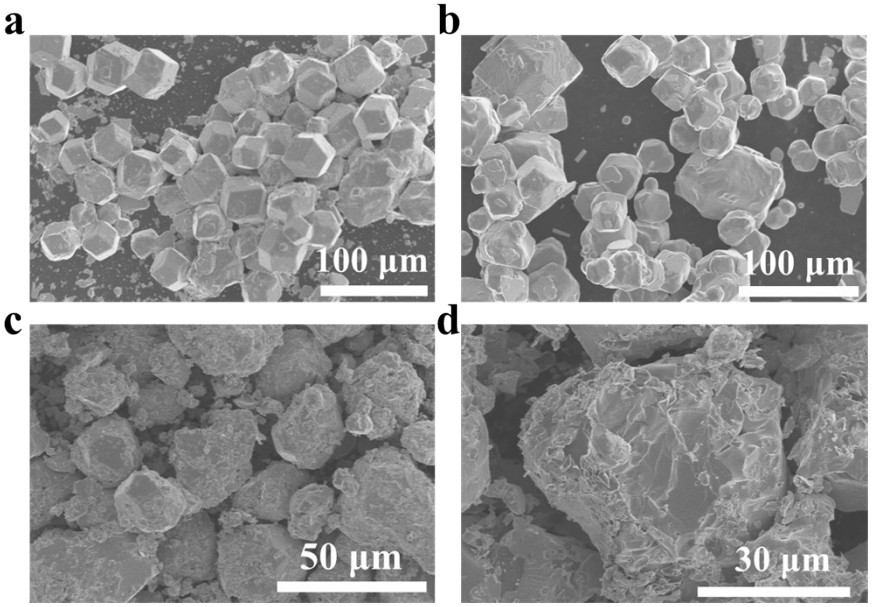

Figure S1. SEM characterizations of the original perovskite and perovskite supported photocatalysts. SEM images for **a**, $FAPbBr_3$. **b**, $FAPbBr_{3-x}I_x$. **c, d**, $Pt/FAPbBr_{3-x}I_x$.

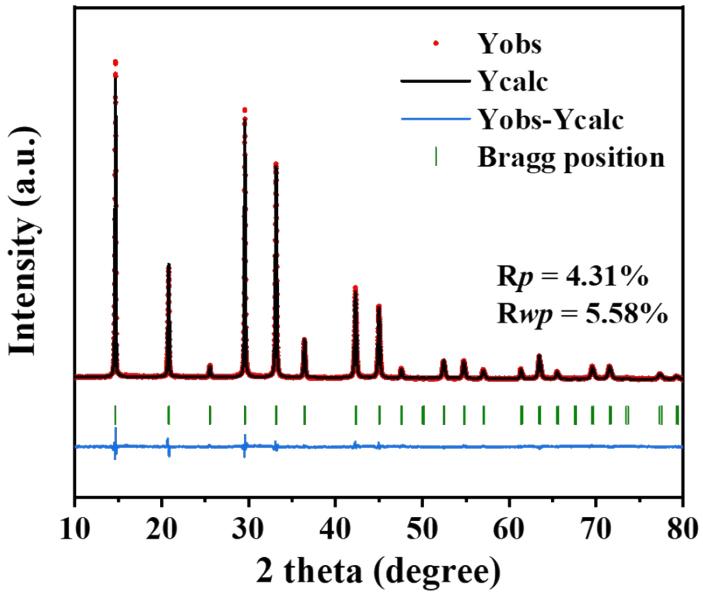

Figure S2. Results of XRD Rietveld refinement.

Rietveld refinement on the powder XRD pattern of $FAPbBr_{2.5}I_{0.5}$, was based on a structure model derived from $FAPbBr_3$ (space group: Pm-3m). Firstly, background was refined by 6-Coefficients polynomial function, and Zero and Cell parameters were refined to determine the peak position. Second, the peak profile and asymmetry were fitted through Pseudo-Voigt function and Berar-Baldinozzi correction, respectively. Subsequently, atomic coordinates were refined. Anisotropic atomic displacement parameters were applied for Pb, Br and I. In terms of the halogen sites (Wyckoff: 3d; 1/2, 0, 0), occupied by Br and I, co-occupied constrains were introduced with the atoms statistically disordered. As a result, reasonable R values were received.

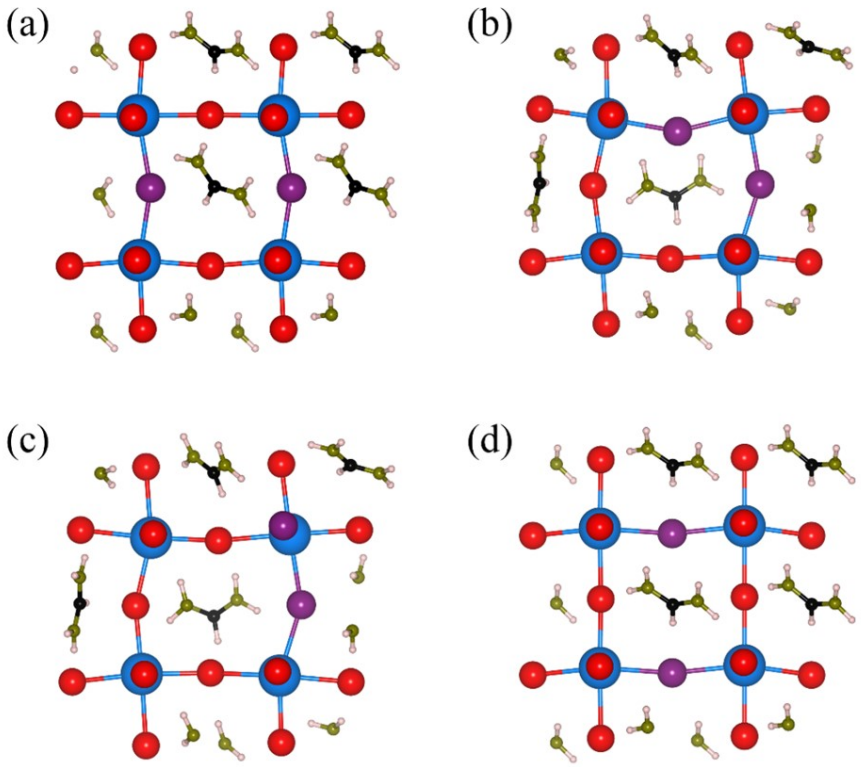

Figure S3. Four built crystal structures of $FAPbBr_{3-x}I_x$ with I replacing different Br. Atoms in blue, red, purple, black, brown, pink represent Pb, Br, I, C, N, H.

Concerning the theoretical simulations, we firstly construct a 2×2×1 supercell of bromide perovskite $FAPbBr_3$, which contains twelve Br atoms. As for the Br substitution for I, we consider the content of I/Br of 1:5 in molar ratio determined by experimental results of EDS measurement and Rietveld refinement of XRD. For direct comparison with experimental results, we replace two Br atoms with two I atoms in the supercell in theoretical calculations, which corresponds to a I/Br ration of 1:5, to determine the most stable substituting configurations of the I atoms in mixed-halide perovskite $FAPbBr_{3-x}I_x$. By considering the crystal symmetry of $FAPbBr_3$, only four configurations can be constructed, as shown in Figure S3. We then calculate the energies of these four systems, and the corresponding energies are shown in Table S2. Obviously, the configuration b is the most stable one, which is lower in energy than the other three configurations of a, c and d, respectively, by 0.428, 0.236 and 0.122 eV. Therefore, we proceed to select the configuration of Fig. S3b for following discussion.

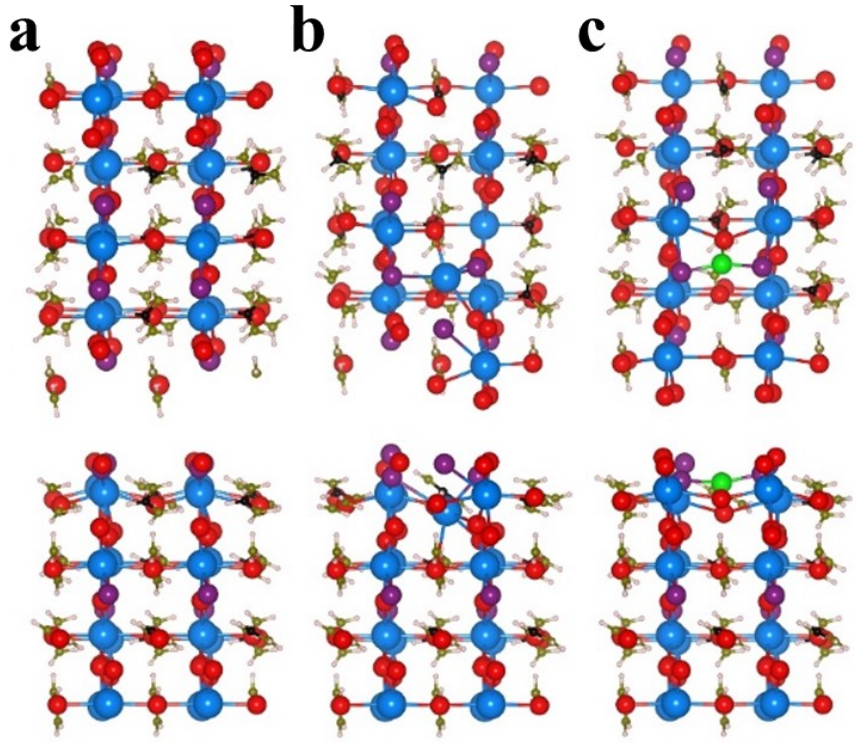

Figure S4. Top (upper) and side (below) view of crystal structures of (a) $FAPbBr_{3-x}I_x$, (b) $FAPbBr_{3-x}I_x$ with FA vacancies, and (c) $FAPbBr_{3-x}I_x$ anchored with Pt single atom respectively for (110) face. Atoms in green, blue, red, purple, black, brown, pink represent Pt, Pb, Br, I, C, N, H.

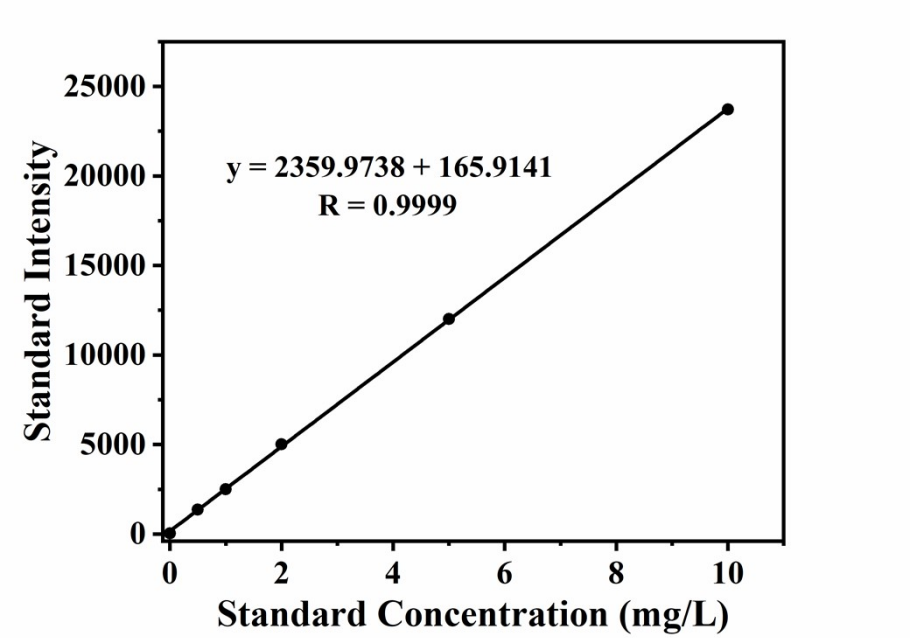

Figure S5. The standard Platinum ion concentration curve for Pt quantification. The corresponding ICP-OES results for Pt loading amounts are listed in **Table S1**.

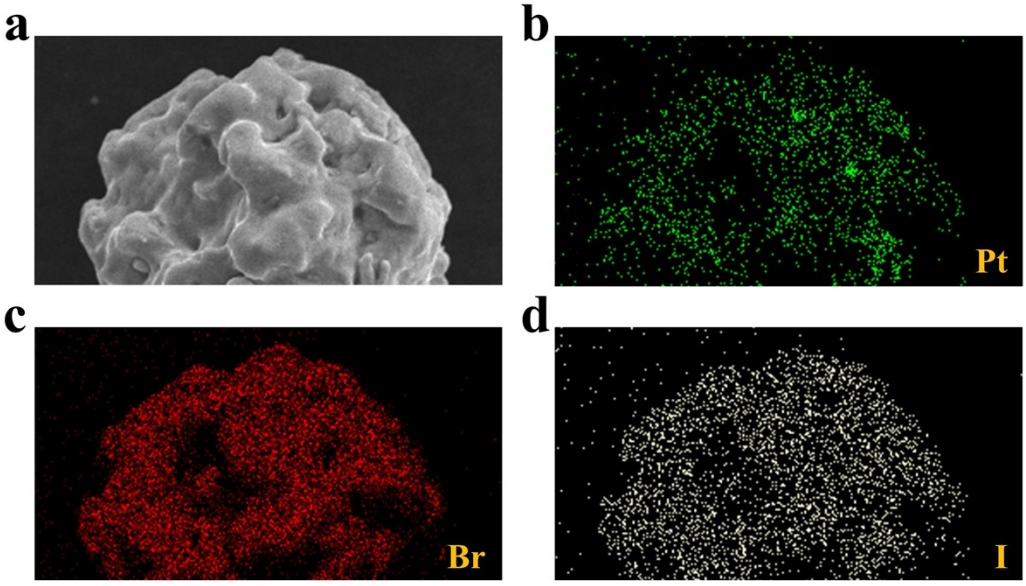

Figure S6. EDS and SEM images of Pt/FAPbBr$_{3-x}$I$_x$.

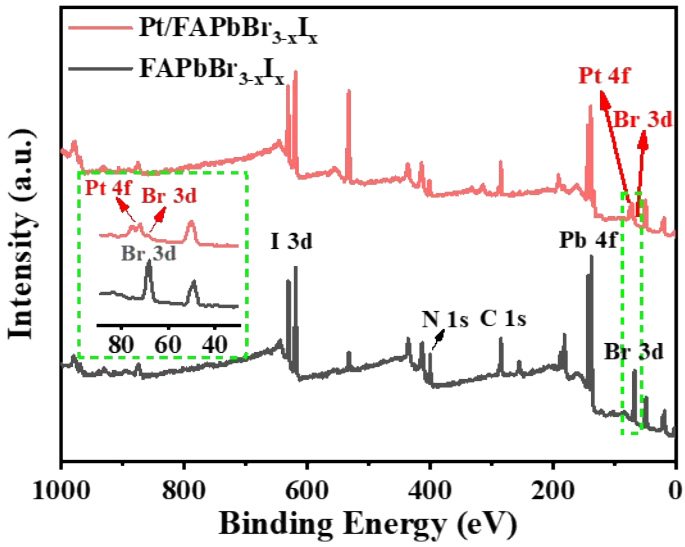

Figure S7. XPS survey spectra of Pt/FAPbBr$_{3-x}$I$_x$ and Pt/FAPbBr$_{3-x}$I$_x$. Inset in green dotted-line: detailed version between the binding energy of 80 and 40 eV.

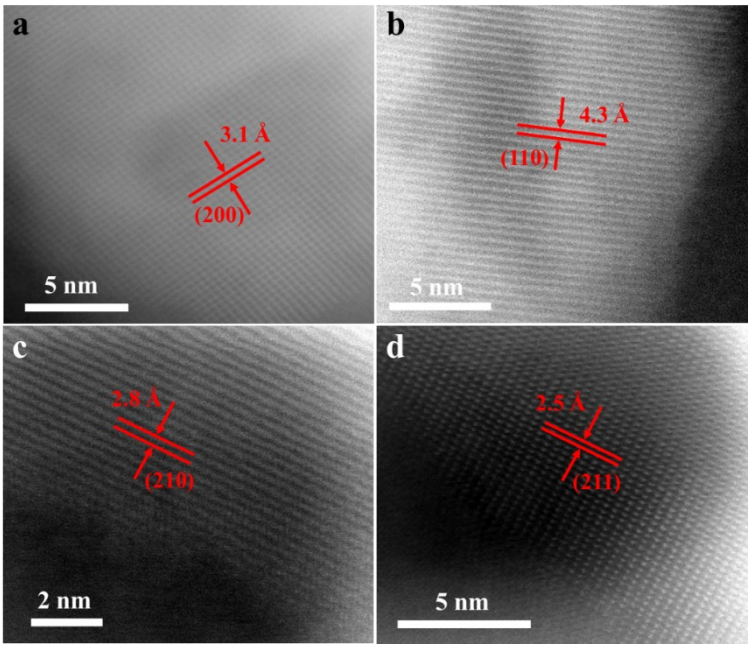

Figure S8. HAADF−STEM images of Pt-loaded perovskite samples. The lattice fringes with different stripe distances clearly show different crystal planes are exposed.

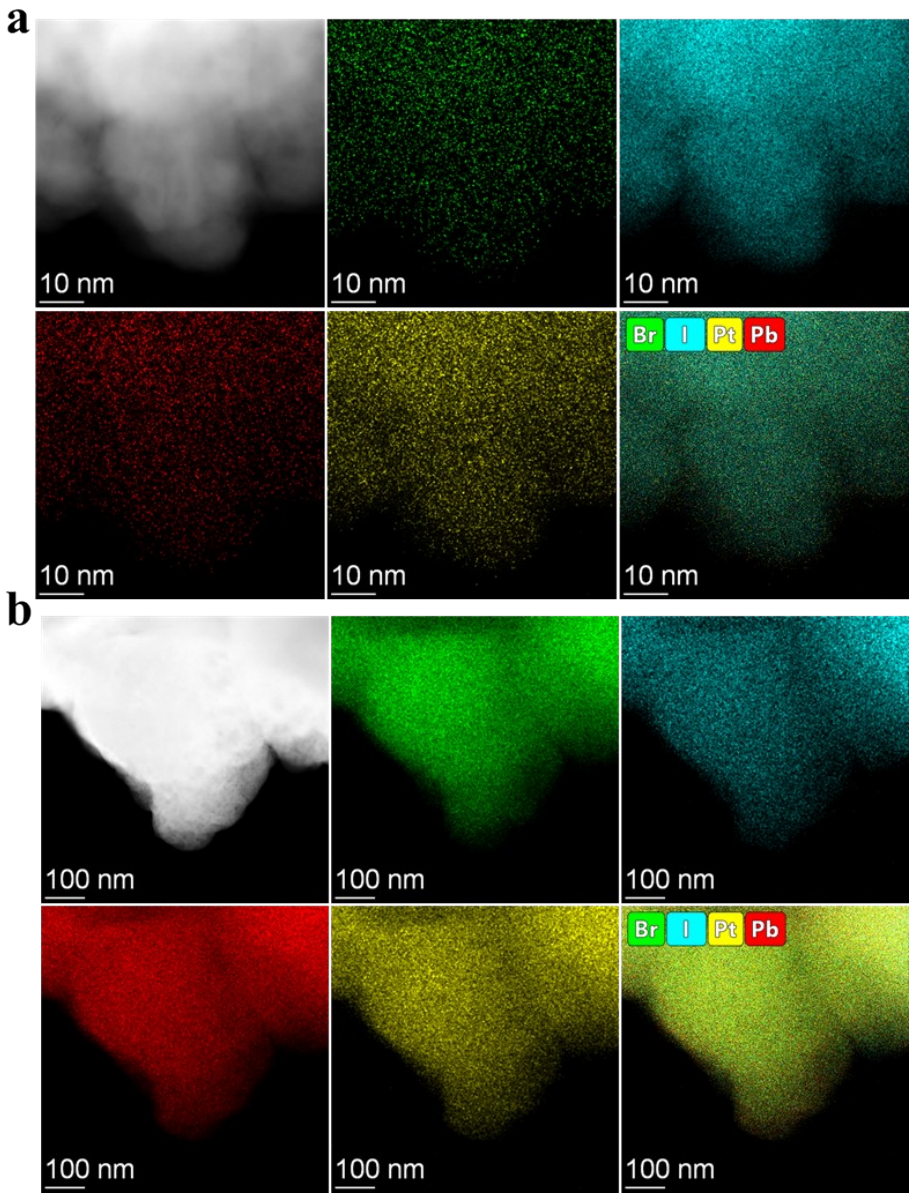

Figure S9. TEM mapping images of Pt/FAPbBr$_{3-x}$I$_x$ samples of two random region.

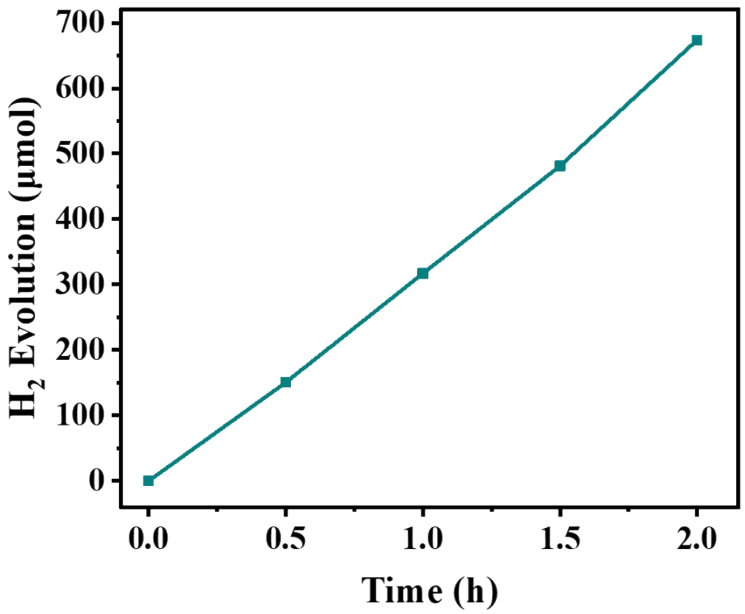

Figure S10. H_2 evolution activity of Pt/$FAPbBr_{3-x}I_3$ under light irradiation through a band-pass filter of 530 nm. The average power energy density of the irradiation light is measured to be 40.32 mW/cm^2.

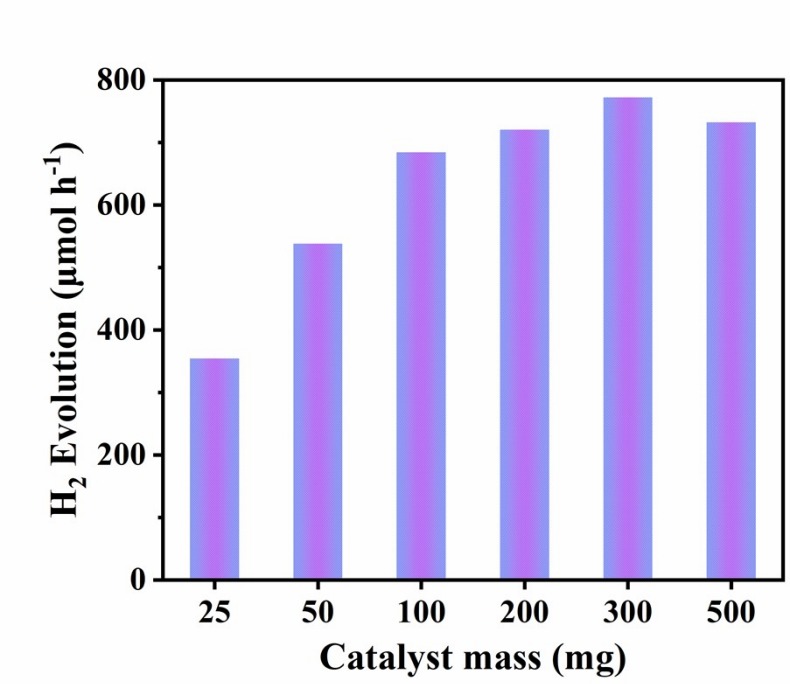

Figure S11. Photocatalytic H_2 evolution using various amounts of Pt/$FAPbBr_{3-x}I_3$ powder.

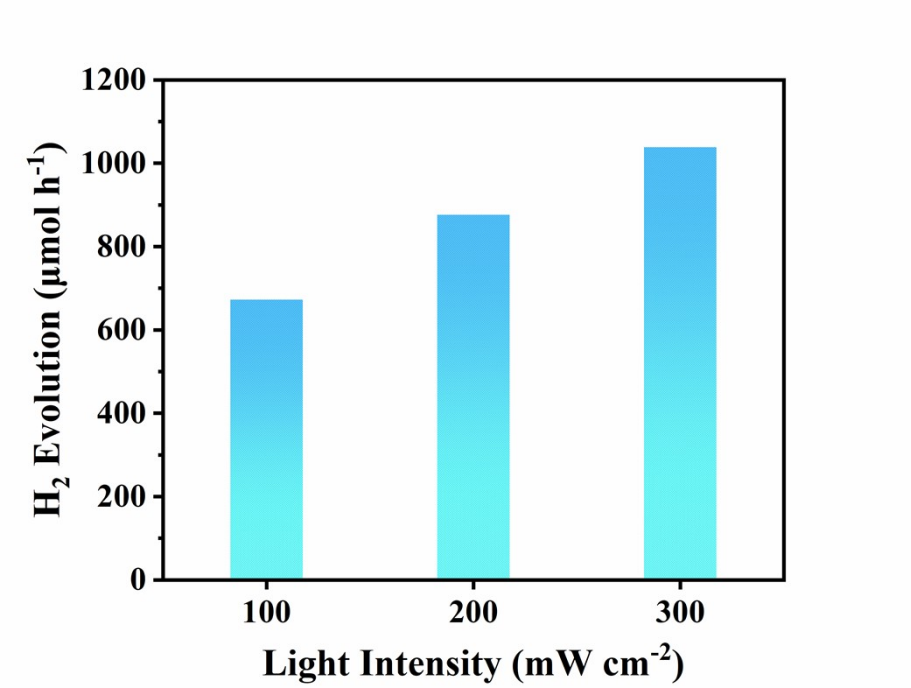

Figure S12. H_2 evolution activities of the 1.8-Pt/$FAPbBr_{3-x}I_x$ perovskite sample under the irradiation of different light intensities.

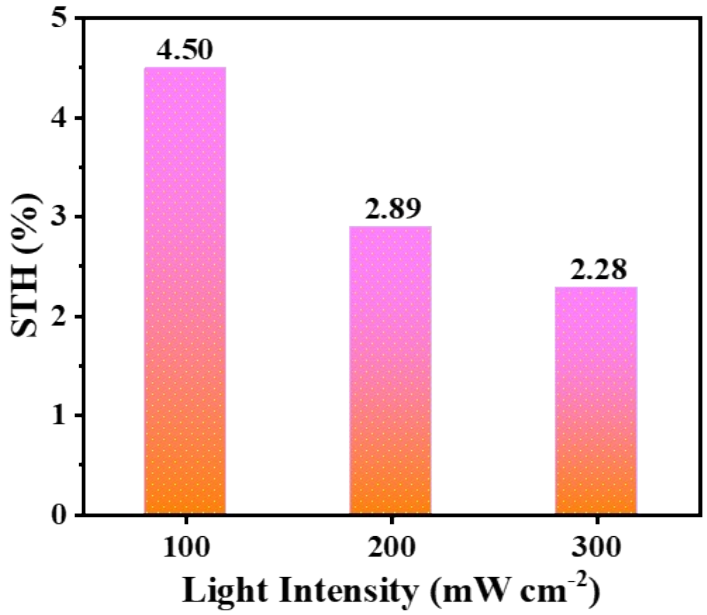

Figure S13. STH of the 1.8-Pt/$FAPbBr_{3-x}I_x$ perovskite sample under the irradiation of different light intensities.

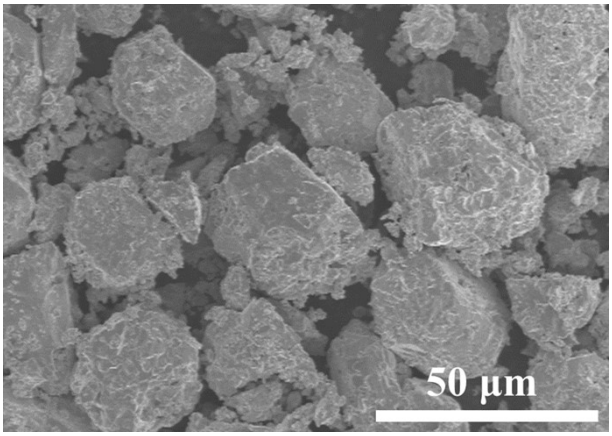

Figure S14. SEM image for Pt/FAPbBr$_{3-x}$I$_x$ after photocatalytic test.

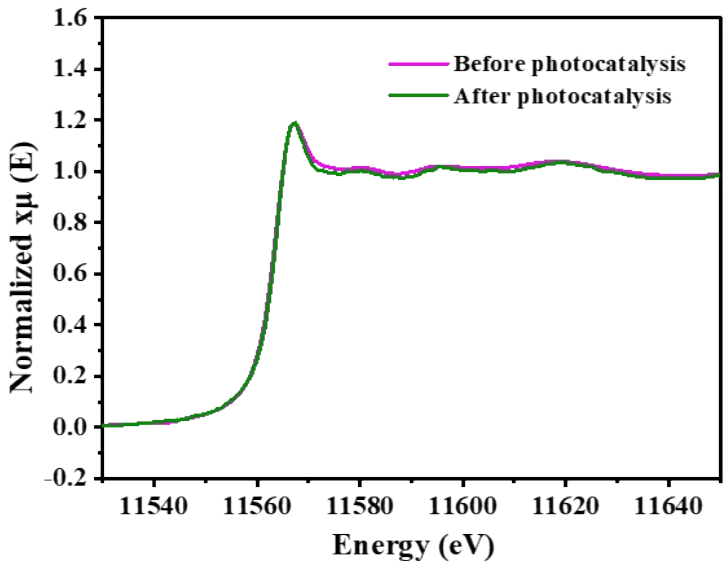

Figure S15. XANES spectra at the Pt L_3-edge of 1.8-Pt/FAPbBr$_{3-x}$I$_x$ after photocatalytic test.

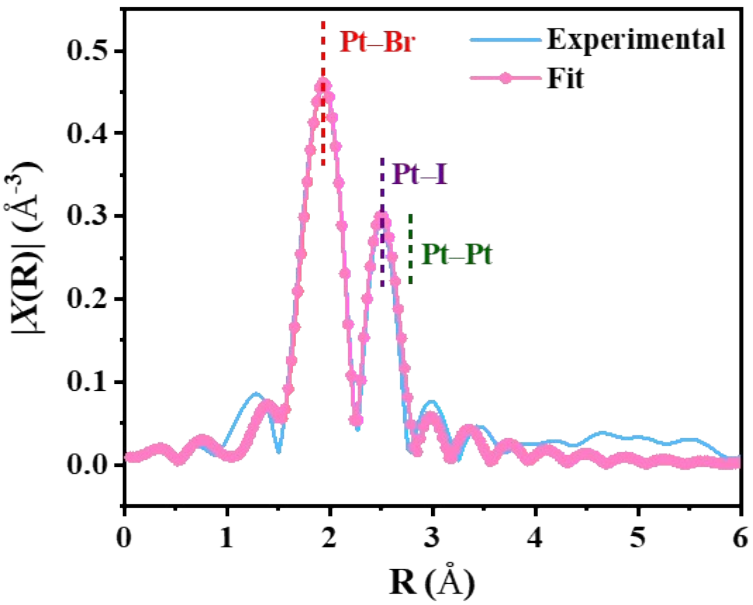

Figure S16. The k_3-weighted Fourier transform spectra from EXAFS.

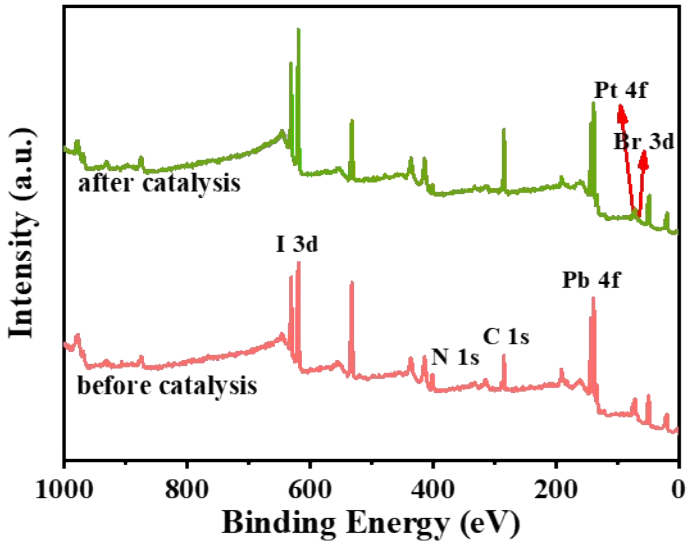

Figure S17. XPS survey spectra of Pt/FAPbBr$_{3-x}$I$_x$ before and after photocatalytic test.

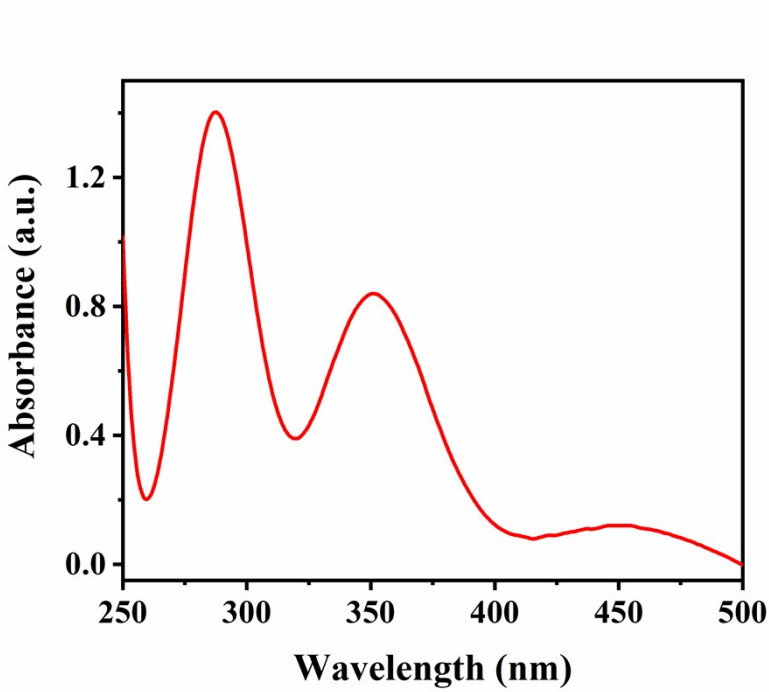

Figure S18. UV-vis light absorption spectrum of HBr/HI aqueous solution used in the sample preparation process and photocatalytic measurement. According to the standard curve of Absorbance vs. concentration of I_3^-, $y = 0.0293x + 0.00299$,[1] the concentration of I_3^- in the current solution is calculated as 4.78×10^{-5} mol L^{-1} .

Table S1. EDS results of element content for $FAPbBr_{3-x}I_x$.

Element	C/N/H	Pb	Br	I	Total
Weight (%)	---	43.6	45.0	11.4	100
Atomic (%)	---	24.6	62.8	12.6	100

Table S2. Total energy of the built configurations of $FAPbBr_{3-x}I_x$ corresponding to the four structures in Fig. S3.

Configuration	a	b	c	d
Energy	–232.855	–233.283	–233.047	–233.161

Table S3. Adsorption energies (eV) of a Pt single atom or a FA molecular on the (110) and (001) surfaces of $FAPbBr_{3-x}I_x$ substrate.

Surface	FA	Pt
(110)	-2.64	-4.54
(001)	-3.24	-6.95

To discuss it more comprehensively, we first construct the (110) and (001) surfaces of $FAPbBr_{3-x}I_x$ substrate, and both surfaces are terminated by the FA. To avoid adjacent interactions, a 2×2 supercell is employed for both surfaces. For the adsorption of Pt single-atom, we first remove one FA from the surface, and then adsorb one Pt atom on vacancy of the two surfaces. Note that the adsorption energy of Pt atom is regarded as a descriptor to determine the structure stability, we calculate the adsorption energy of Pt atom on the $FAPbBr_{3-x}I_x$ substrate according to the formula $E_{Pt\text{-}ad} = E_{*Pt} - E_{va} - E_{Pt}$. Here, E_{*Pt} is the total energy of Pt-adsorbed substrate, E_{va} is the energy of the substrate with a single FA vacancy and E_{Pt} is the energy of Pt single atom. For comparison, we further calculate the binding energy of $FAPbBr_{3-x}I_x$ substrate with respect to FA molecule and $FAPbBr_{3-x}I_x$ substrate with one single FA vacancy following the formula $E_{FA\text{-}b} = E_{*FA} - E_{va} - E_{FA}$. Here, E_{*FA} is the total energy of $FAPbBr_{3-x}I_x$ substrate and E_{FA} is the energy of single FA molecule.

Table S4. The Pt loading amount of the samples measured by ICP-OES

Sample	2Pt-FPBI	4Pt-FPBI	6Pt-FPBI	8Pt-FPBI	10Pt-FPBI
Pt loading (wt%)	0.71	1.15	1.51	1.80	2.12

The items in the first raw named "*x*Pt-FPBI", in which the "*x*" represents the mass of $H_2PtCl_6 \cdot 6H_2O$ added in the synthetic solution.

Table S5. FT EXAFS fitting results of Pt/$FAPbBr_{3-x}I_x$, and Pt foil and $H_2PtCl_6 \cdot 6H_2O$ are given as references.

	Path	CN	R(Å)	ΔE_0(eV)	σ^2(10^3 Å^2)	R factor
Pt-foil	Pt-Pt	12	2.76±0.004	8.35±0.79	4.20±0.56	0.004
Pt/OHP	Pt-Br	0.86±0.19	2.46±0.016	11.92±2.43	8.60±1.92	0.009
	Pt-I	1.30±0.32	2.58±0.022	6.08±1.76	4.99±1.96	
$H_2PtCl_6 \cdot 6H_2O$	Pt-Cl	6	2.31±0.006	9.97±0.95	2.98±0.16	0.004

CN is coordination numbers of identical atoms; R is interatomic distance; ΔE_0 is energy shift; σ^2 is Debye-Waller factors; R factor is goodness of fit. The data range used for data fitting in k-space (Δk) and R-space (ΔR) are 3.0–11.5 Å^{-1} and 1.0–4.0 Å, respectively.

Table S6. A summary of the performance and experimental parameters of reported halide perovskite photocatalysts for H_2 evolution

Catalysts	Mass of catalyst (mg)	Light source	Irradiation area (cm^2)	Activity ($\mu mol\ h^{-1}$)	STH (%)	Year/ref.
Pt/FAPbBr$_{3-x}$I$_3$	**100**	**AM 1.5G, 100 mW cm^{-2}**	**π**	**682.6**	**4.50**	**This work**
MAPbI$_3$/Pt	200	λ > 475 nm, 100 mW cm^{-2}	0.25	11.4	0.81	2016[1]
MAPbI$_3$/rGO	100	λ ≥ 420 nm, 120 mW cm^{-2}	18.1	93.9	--	2018[2]
MAPbI$_3$-Pt/TiO$_2$	50	λ > 420 nm 200 mW cm^{-2}	1.82	89.2	0.86	2018[3]
MAPbBr$_{3-x}$I$_x$/Pt	250	AM 1.5G, 100 mW cm^{-2}	π	161.5	1.05	2018[4]
Ni$_3$C/MAPbI$_3$	50	λ ≥ 420 nm, 100 mW cm^{-2}	0.25	--	0.91	2019[5]
MAPbI$_3$/BP	30	λ ≥ 420 nm, 100 mW cm^{-2}	0.25	--	0.93	2019[6]
Cs$_3$Bi$_{0.6}$Sb$_{1.4}$I$_9$	100	AM 1.5G, 100 mW cm^{-2}	16π	92.6	0.32	2020[7]
ML-MoS$_2$/MAPbI$_3$	100	AM 1.5G, 60 mW cm^{-2}	16.6	637	1.09	2020[8]
Pt/MAPbI$_3$/ CA-PASA	100	λ ≥ 420 nm, 100 mW cm^{-2}	0.25	--	2.15	2020[9]
Pt/2D-PMA$_2$PbI$_4$	150	AM 1.5G, 100 mW cm^{-2}	2	120	1.57	2021[10]

Note: the activities and irradiation area listed in the table are the data used for STH calculation in the corresponding papers.

Table S7. PL decay fitting results of samples $FAPbBr_{3-x}I_x$ and $Pt/FAPbBr_{3-x}I_x$.

Sample	A_1	τ_1 (ns)	A_2	τ_2 (ns)	τ (ns)	$\tau_{average}$ (ns)
a1	3.99	130.36	-2.92	112.00	161.62	104.12
a2	0.34	7.43	0.47	59.94	55.57	
a3	2.76	94.16	-1.95	93.73	95.17	
b1	0.92	0.52	0.11	0.52	0.52	0.44
b2	0.83	0.36	0.18	0.36	0.36	
b3	0.82	0.45	0.19	0.45	0.45	

Note: the fitting function used here is: $y = A_1*\exp(-x/\tau_1) + A_2*\exp(-x/\tau_2) + y_0$.

References

1. S. Park, W. J. Chang, C. W. Lee, S. Park, H.-Y. Ahn and K. T. Nam, *Nat. Energy*, 2016, **2**, 16185.
2. Y. Wu, P. Wang, X. Zhu, Q. Zhang, Z. Wang, Y. Liu, G. Zou, Y. Dai, M. H. Whangbo and B. Huang, *Adv. Mater.*, 2018, **30**, 1704342.
3. X. Wang, H. Wang, H. Zhang, W. Yu, X. Wang, Y. Zhao, X. Zong and C. Li, *ACS Energy Lett.*, 2018, **3**, 1159–1164.
4. Y. Wu, P. Wang, Z. Guan, J. Liu, Z. Wang, Z. Zheng, S. Jin, Y. Dai, M.-H. Whangbo and B. Huang, *ACS Catal.*, 2018, **8**, 10349–10357.
5. Z. Zhao, J. Wu, Y.-Z. Zheng, N. Li, X. Li and X. Tao, *ACS Catal.*, 2019, **9**, 8144–8152.
6. R. Li, X. Li, J. Wu, X. Lv, Y.-Z. Zheng, Z. Zhao, X. Ding, X. Tao and J.-F. Chen, *Appl. Catal. B*, 2019, **259**, 118075.
7. G. Chen, P. Wang, Y. Wu, Q. Zhang, Q. Wu, Z. Wang, Z. Zheng, Y. Liu, Y. Dai and B. Huang, *Adv. Mater.*, 2020, **32,** 2001344.
8. X. Zhao, S. Chen, H. Yin, S. Jiang, K. Zhao, J. Kang, P. F. Liu, L. Jiang, Z. Zhu, D. Cui, P. Liu, X. Han, H. G. Yang and H. Zhao, *Matter*, 2020, **3,** 1–15.
9. Y. Zhao, Q. Zeng, Y. Yu, T. Feng, Y. Zhao, Z. Wang, Y. Li, C. Liu, J. Liu, H. Wei, S. Zhu, Z. Kang, H. Zhang and B. Yang, *Materials Horizons*, 2020, **7**, 2719–2725.
10. H. Wang, H. Zhang, J. Wang, Y. Gao, F. Fan, K. Wu, X. Zong and C. Li, *Angewandte Chemie*, 2021, **60**, 7376–7381..